Vacuum stability in rotating spacetimes

Corinne A. Manogue*
Center for Relativity, The University of Texas at Austin, Austin, Texas 78712
(Received 6 February 1987)

Just as the mere presence of boundaries can create a change in the vacuum expectation value of the stress tensor (the Casimir effect), so can the rotation of such boundaries. Calculations of the Casimir effect are made for a massless scalar field confined to an infinitely long square box. A comparison is made with the results of other authors for the Casimir effect near flat planes and inside angles. The change in the vacuum expectation value of the momentum density is calculated for this same box rotating around its long central axis. An estimate is made of the moment of inertia per unit length for the rotating box.

I. INTRODUCTION

In 1948 Casimir[1] made his famous prediction that two perfectly conducting parallel plates should experience a mutual attractive force

$$F=0.013\frac{1}{a^4}\ \text{dyn/cm}^2\ ,$$

where a is the distance between the plates, measured in microns. This force comes from the change in the zero-point energy of the electromagnetic field due to the presence of the plates. In 1958 this force was measured in the Philips Research Laboratories by Sparnaay,[2] physical confirmation that the idea of vacuum energy must be taken seriously. Since that time the Casimir effect, a name applied to changes both in the total energy and in the vacuum expectation value of the stress-energy tensor, due to the presence of surfaces, has been calculated for a number of different physical situations. (For example, inside angles,[3] inside variously shaped cavities,[4] near arbitrarily curved surfaces,[5] near dielectrics,[6] and for accelerating boundaries.[7])

Moving boundaries are particularly interesting. Of course due to Lorentz invariance there are no physically measurable differences between a boundary moving rigidly with constant velocity and the same boundary at rest. Cases of linear acceleration have been thoroughly investigated.[7] They show changes in the stress-energy tensor far from the boundary, corresponding to a thermal bath of particles [with temperature $T=(2\pi\xi)^{-1}$, where ξ^{-1} is the proper acceleration of the boundary] missing from the vacuum in the presence of an accelerating boundary, relative to the vacuum without this boundary.

It is the purpose of this paper to consider the case of rotating boundaries. Letaw and Pfautsch[8] have shown that an observer orbiting a point in flat, unbounded Minkowski space observes a spectrum of vacuum fluctuations over and above that expected from his acceleration, indicating that a vacuum state might exist tailored to rotating boundary conditions. The difficulty has been to find modes appropriate to rotating boundaries. In one simple case, that of a rotating cylinder of radius R, the modes are identical to those for a nonrotating cylinder. Therefore the vacuum expectation values of the stress-energy tensors will be identical for these two cases. Some confusion in the past has resulted because the frequency spectrum is shifted downward in the rotating case relative to the nonrotating case, i.e., in the nonrotating case the modes are

$$\phi=\frac{1}{2\pi R\,|J_{m+1}(x_{mn})|\,\omega^{1/2}}J_m\left[\frac{x_{mn}r}{R}\right]e^{i(m\theta+kz)}e^{-i\omega t}$$

and in the rotating case they are

$$\phi=\frac{1}{2\pi R\,|J_{m+1}(x_{mn})|\,\omega^{1/2}}\times J_m\left[\frac{x_{mn}r}{R}\right]e^{i(m\theta+kz)}e^{-i(\omega-m\Omega)t}\ ,$$

where

$$\omega^2=k^2+\frac{x_{mn}{}^2}{R^2}\ , \tag{1}$$

Ω is the angular velocity of the cylinder, and x_{mn} is the nth zero of the Bessel function $J_m(z)$. (The differences can be shown to be just a change from nonrotating to rotating coordinates.) It was assumed that some of the positive-frequency modes $\omega>0$ in the nonrotating case would become negative-frequency modes $\omega-m\Omega<0$ in the rotating case. This could cause differences in the vacuum expectation values of operators since some of the modes which had positive norm corresponding to particle states would now have negative norm corresponding to antiparticle states, forcing a change from annihilation operators to creation operators in the quantization procedure. However Pfautsch showed that by the condition[9]

$$x_{mi}>m$$

on the zeros of Bessel functions and Eq. (1), one obtains

$$\omega^2\geq\frac{m^2}{R^2}\geq m^2\Omega^2$$

whenever $R\Omega<1$. But this is just the condition that the boundary rotate at less than the speed of light. Thus we see that for physically reasonable situations ω is always

greater than $m\Omega$. The shift in frequency does not change any positive-frequency modes to negative-frequency modes. The anticipated difficulty does not arise. The case of a rotating cylinder is uninteresting in that the vacuum cannot tell that smooth cylindrical walls are rotating. Hence we are led to consider rotating boundaries of other shapes with "roughness" to "push" the vacuum around. Unfortunately the field equations for rotating boundaries with other shapes have thus far proven insoluble. This paper avoids the problem by calculating a perturbation expansion for the appropriate Green's function to first order in the angular velocity of the boundary.

It has been shown in other examples[5] that the conformally coupled stress-energy tensor for the massless scalar field shows many of the same qualitative features as the physically relevant electromagnetic field. Therefore for simplicity a massless scalar field is used throughout this paper. Results for both the conformally coupled and the minimally coupled stress-energy tensor are given. Both Dirichlet and Neumann boundary conditions are used.

In Sec. II the Casimir effect in an infinitely long box with square cross section is calculated using Green's-function techniques and the method of images. The result is evaluated numerically. A comparison is made with the results of other authors for the stress-energy tensor near flat planes and inside angles. In Sec. III Green's-function techniques are used to calculate the correction, to first order in the angular velocity, for the vacuum expectation value of the stress-energy tensor when the box is rotating. Only the momentum density acquires a first-order correction. The results are evaluated numerically. An estimate is made of the moment of inertia per unit length for a rotating box.

II. THE NONROTATING BOX

The Feynman Green's function for a massless scalar field is a solution of

$$FG(x,x')=-g^{-1/2}\delta^4(x,x')\ ,$$

where $F=g^{-1/2}\partial_\mu g^{1/2}g^{\mu\nu}\partial_\nu$ and $g=-\det(g_{\mu\nu})$. The boundary conditions for $G(x,x')$ used in this paper are Dirichlet [$G_D(x,x')=0$ for x or x' on the boundary of the spacetime] and Neumann [the normal derivative of $G_N(x,x')=0$ for x or x' on the boundary of the spacetime]. In flat, nonrotating space, we use $g_{\mu\nu}=\eta_{\mu\nu}=\mathrm{diag}(-1,1,1,1)$. The vacuum expectation value of the stress-energy tensor is given by

$$\langle 0\,|\,T^{\mu\nu}\,|\,0\rangle_{D,N}=\lim_{x'\to x}\left[-\left(\tfrac{1}{2}-2\xi\right)(g^{\mu\nu}g^{\rho\sigma'}D_\rho D_{\sigma'})+\tfrac{1}{2}(1-2\xi)(g^{\mu\rho}g^{\nu\sigma'}+g^{\mu\sigma'}g^{\nu\rho})(D_\rho D_{\sigma'})\right.$$
$$\left.-\xi(g^{\mu\rho'}g^{\nu\sigma'}D_{\rho'}D_{\sigma'}+g^{\mu\rho}g^{\nu\sigma}D_\rho D_\sigma)\right](-i)G_{D,N}(x,x')\ , \tag{2}$$

where $g^{\mu\nu'}$ is the bivector of parallel transport (which transports vectors from the point x' to the point x via parallel propagation along the geodesic joining x' with x). $\xi=\frac{1}{6}$ for the conformally coupled scalar field and $\xi=0$ for the minimally coupled scalar field.

For the original Casimir case of two infinitely broad parallel plates separated by a distance a in the x direction, the Green's function is

$$G_{D,N}(x,x')=\frac{i}{4\pi^2}\sum_{n=-\infty}^{\infty}(\mp 1)^n\frac{1}{-(t-t')^2+[x-(-1)^n x'+na]^2+(y-y')^2+(z-z')^2+i\epsilon}\ ,$$

where the top sign corresponds to Dirichlet boundary conditions and the bottom sign to Neumann (a convention which will be followed throughout the paper). Notice that the term with $n=0$ is the usual Minkowski Green's function and the other terms are the contributions from the image of the original source x', formed by multiple reflections in the walls. See Fig. 1. The Green's function is renormalized by subtracting the ordinary Minkowski term. A straightforward calculation for the renormalized stress-energy tensor gives[10]

$$\langle 0\,|\,T^{\mu\nu}\,|\,0\rangle_{D,N}=\frac{\pi^2}{1440a^4}\mathrm{diag}(-1,-3,1,1)$$

for the conformally coupled case and

$$\langle 0\,|\,T^{\mu\nu}\,|\,0\rangle_{D,N}=\frac{\pi^2}{1440a^4}\mathrm{diag}(-1,-3,1,1)\mp\frac{\pi^2}{48a^4}\frac{3-2\sin^2\left[\pi\left[\frac{x}{a}+\frac{1}{2}\right]\right]}{\sin^4\left[\pi\left[\frac{x}{a}+\frac{1}{2}\right]\right]}\mathrm{diag}(-1,0,1,1)$$

for the minimally coupled case. Notice that in the conformally coupled case the components of the stress-energy tensor are constant between the plates, while in the minimally coupled case some of the components blow up as the distance from the plate to the inverse fourth power. Brown and Maclay[11] have shown that the electromagnetic field also gives a stress-energy tensor which is constant between the plates

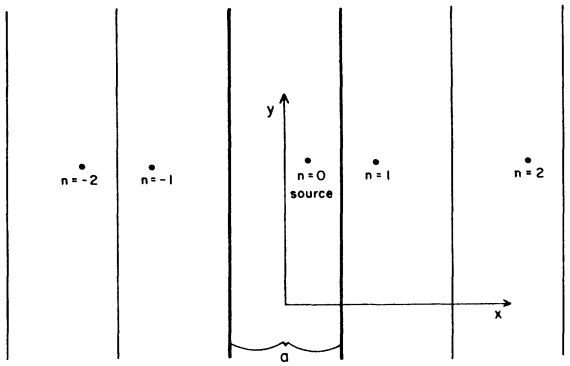

FIG. 1. Images for the Green's function between two parallel plates separated by a distance a.

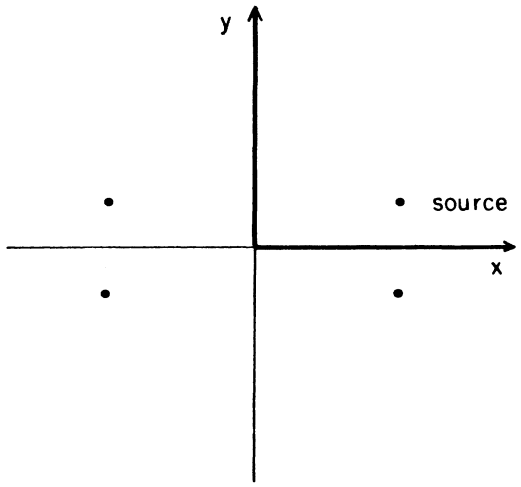

FIG. 2. Images for the Green's function inside a right angle.

$$\langle 0 \mid T^{\mu\nu} \mid 0 \rangle_{\mathrm{EM}} = \frac{\pi^2}{720a^4}\,\mathrm{diag}(-1,-3,1,1)$$

and Deutsch and Candelas[5] have shown that in general it has the same qualitative behavior near boundaries as the conformally coupled scalar field. Therefore the results in this paper for the conformally coupled scalar field can be expected to give the best predictions for the behavior of the electromagnetic field. The results for the minimally coupled scalar field are presented for completeness.

Deutsch and Candelas have also shown that unbounded behavior of components of the stress-energy tensor is the generic situation for all three fields near curved boundaries (including moving boundaries as a generalization with space-*time* curvature), and have calculated the general form for the divergences near such a curved boundary. These divergences appear because of the imposition of perfect-conductor-type boundary conditions. Boundaries made of real physical materials would not look like perfect conductors for arbitrarily high frequencies and a cutoff depending on the molecular details of the boundary material should be imposed. This is not however a reason for throwing out these divergences altogether. The cutoff would ordinarily be at lengths significantly smaller than any length scale (such as the plate separation a) imposed by the problem. In this case the components of the stress-energy tensor become quite large near the boundary.

The divergences in $\langle 0 \mid T^{\mu\nu} \mid 0 \rangle$ near boundaries arise because $G(x,x')$ is infinite as x' approaches x. The overall divergence as x approaches the original source term is just the usual divergence from the Minkowski Green's function and is thrown away in the renormalization procedure, but divergent terms on the boundaries remain. If the problem is solved by the method of images, the physical meaning of these terms is clear; a divergence can be expected from the image formed by a single reflection in the boundary in the limit as the point x and the image both approach that boundary. In the parallel-plate calculation above, for the conformally coupled scalar field, the images formed from an odd number of reflections in the plates, henceforth called odd-numbered images, do not contribute to $\langle 0 \mid T^{\mu\nu} \mid 0 \rangle$ because of delicate cancellations due to the symmetries in the problem, and hence the components are finite as the boundary is approached. These cancellations do not occur if there is even a slight curvature in the boundary or in the minimally coupled case; nor do they occur for $\langle E^2 \rangle$ or $\langle H^2 \rangle$, and hence the Lamb shift is modified even near flat boundaries.

The only difference between the Green's functions for Dirichlet and Neumann boundary conditions is an overall sign change in terms from the odd-numbered images. Since these terms do not contribute in the conformally coupled case above, there is no difference between

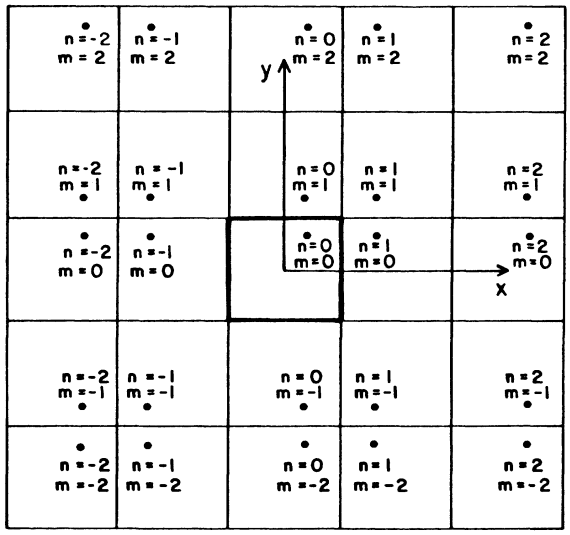

FIG. 3. Images for the Green's function inside an infinitely long nonrotating box with side of length a.

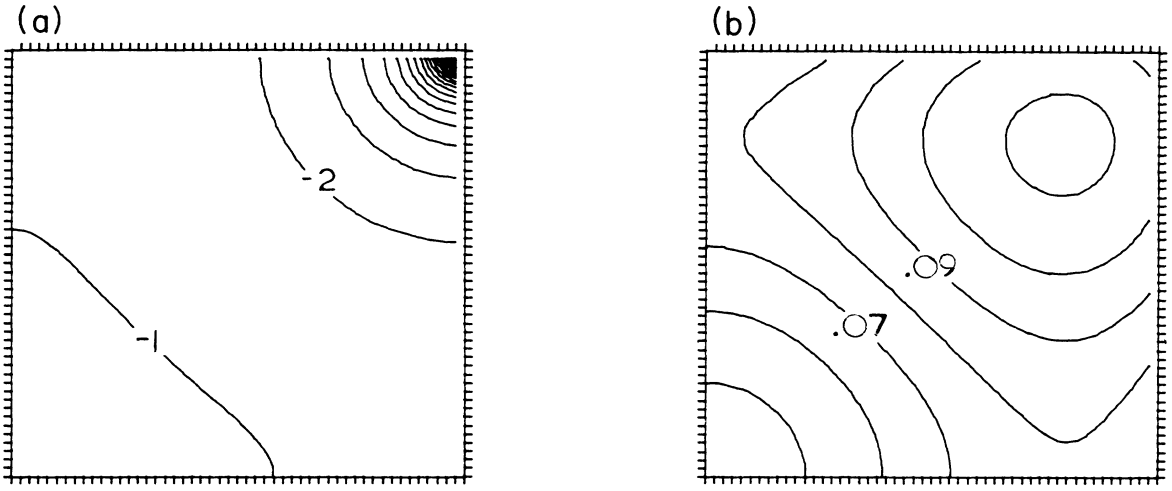

FIG. 4. (a) The vacuum expectation value of the energy density $\langle 0 | T^{tt} | 0 \rangle$ for the conformally coupled massless scalar field, satisfying Dirichlet boundary conditions, confined inside an infinitely long nonrotating box with side of length a, centered at the origin. Actually graphed is a contour plot of the fourth root of the vacuum expectation value in units of $1/4\pi^2 a^4$ for the upper right-hand quadrant of a cross section of the box ($0 \le x \le a/2$, $0 \le y \le a/2$, $z = 0$). The entire cross section can be obtained by reflection in the x and/or y axes. (b) As in (a) but with the divergent edge and corner contributions subtracted.

$\langle 0 | T^{\mu\nu} | 0 \rangle_D$ and $\langle 0 | T^{\mu\nu} | 0 \rangle_N$. In the minimally coupled case, the divergence near the boundary is caused by the images from a single reflection. Thus the divergent term differs by an overall sign for the two boundary conditions.

The Green's function for a right angle with edges along the x and y axes has four terms: the original Minkowski term and three image terms (see Fig. 2)

$$G_{D,N}(x,x') = \frac{i}{4\pi^2}\left[\frac{1}{-(t-t')^2+(x-x')^2+(y-y')^2+(z-z')^2+i\epsilon} \mp \frac{1}{-(t-t')^2+(x+x')^2+(y-y')^2+(z-z')^2+i\epsilon}\right.$$

$$\left. \mp \frac{1}{-(t-t')^2+(x-x')^2+(y+y')^2+(z-z')^2+i\epsilon} + \frac{1}{-(t-t')^2(x+x')^2+(y+y')^2+(z-z')^2+i\epsilon}\right]$$

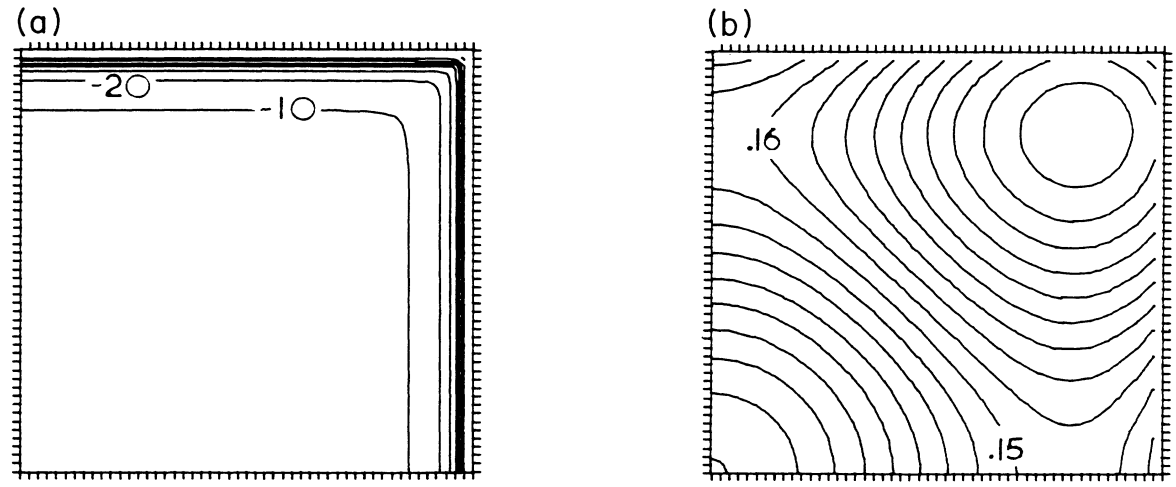

FIG. 5. As in Fig. 4, but for $\langle 0 | T^{tt} | 0 \rangle$ for the minimally coupled field satisfying Dirichlet boundary conditions.

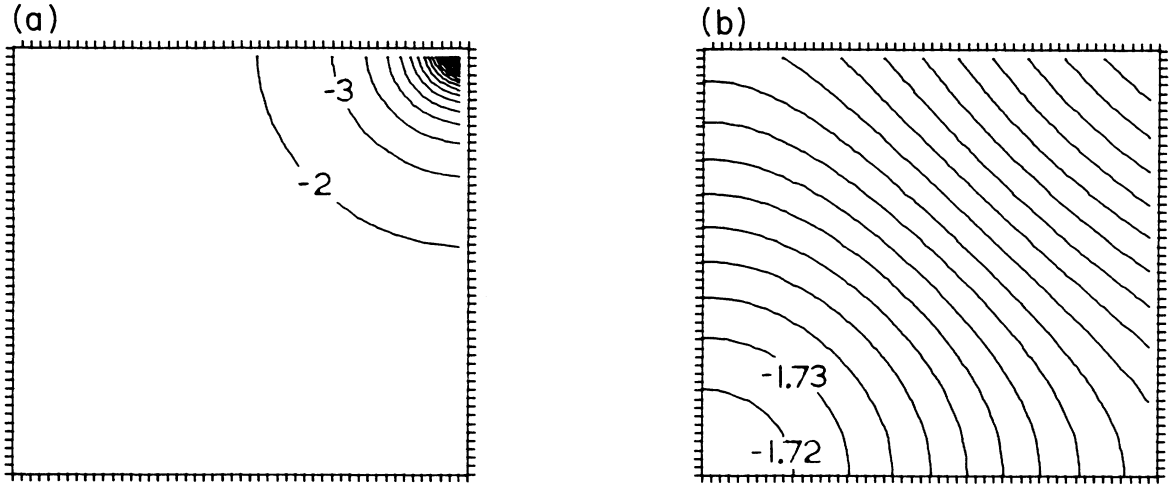

FIG. 6. As in Fig. 4, but for $\langle 0 \mid T^{\mu} \mid 0 \rangle$ for the conformally coupled field satisfying Neumann boundary conditions.

leading to[3]

$$\langle 0 \mid T^{\mu\nu} \mid 0 \rangle_{D,N} = \frac{1}{96\pi^2} \begin{bmatrix} \frac{-1}{(x^2+y^2)^2} & 0 & 0 & 0 \\ 0 & \frac{x^2-3y^2}{(x^2+y^2)^3} & \frac{4xy}{(x^2+y^2)^3} & 0 \\ 0 & \frac{4xy}{(x^2+y^2)^3} & \frac{-3x^2+y^2}{(x^2+y^2)^3} & 0 \\ 0 & 0 & 0 & \frac{1}{(x^2+y^2)^2} \end{bmatrix}$$

in the conformally coupled case and

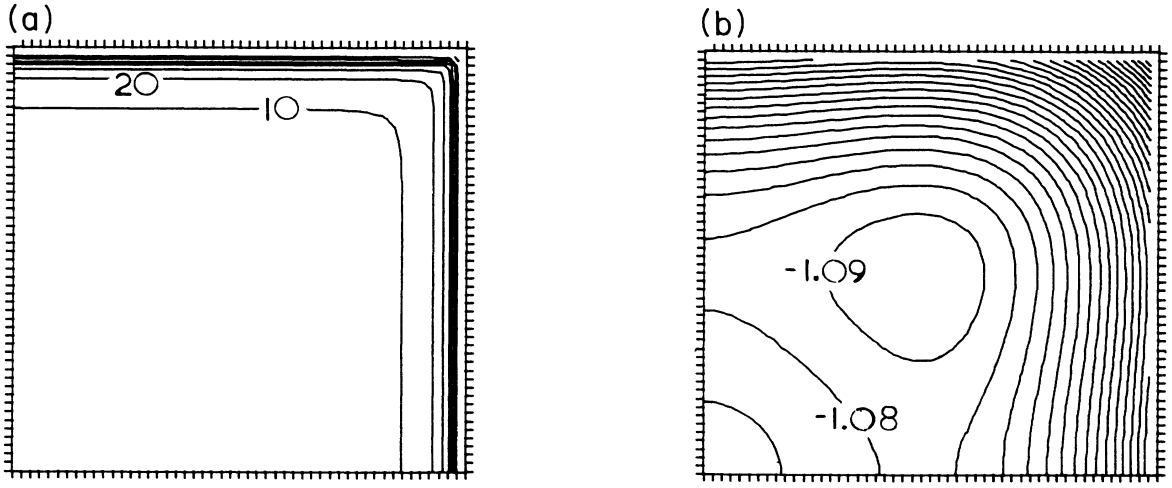

FIG. 7. As in Fig. 4, but for $\langle 0 \mid T^{\mu} \mid 0 \rangle$ for the minimally coupled field satisfying Neumann boundary conditions.

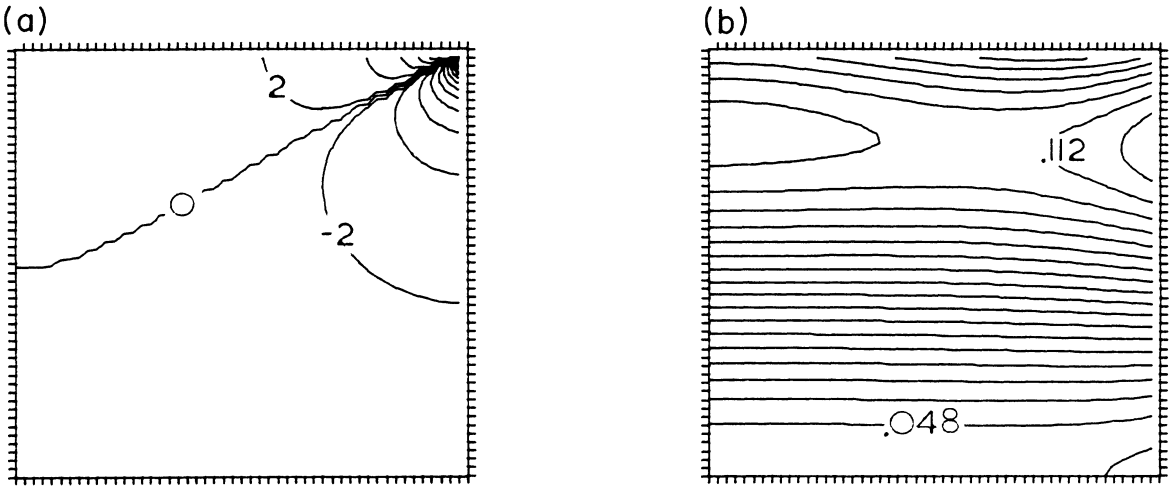

FIG. 8. As in Fig. 4, but for $\langle 0 \mid T^{xx} \mid 0 \rangle$ for the conformally coupled field satisfying Dirichlet boundary conditions.

$$\langle 0 \mid T^{\mu\nu} \mid 0 \rangle_{D,N} = \frac{1}{32\pi^2} \begin{pmatrix} \frac{1}{(x^2+y^2)^2} \mp \frac{2}{x^4} \mp \frac{2}{y^4} & 0 & 0 & 0 \\ 0 & \frac{x^2-3y^2}{(x^2+y^2)^3} \pm \frac{2}{y^4} & \frac{4xy}{(x^2+y^2)^3} & 0 \\ 0 & \frac{4xy}{(x^2+y^2)^3} & \frac{-3x^2+y^2}{(x^2+y^2)^3} \pm \frac{2}{x^4} & 0 \\ 0 & 0 & 0 & -\frac{1}{(x^2+y^2)^2} \pm \frac{2}{x^4} \pm \frac{2}{y^4} \end{pmatrix}$$

in the minimally coupled case. Again the odd-numbered images cancel in the conformally coupled case but the third image causes a divergence which varies inversely as the distance from the corner to the fourth power. The minimally coupled case shows both the edge and corner divergences.

The Green's function for an infinitely long box with square cross section is

$$G_{D,N}(x,x') = \frac{i}{4\pi^2} \sum_{n=-\infty}^{\infty} \sum_{m=-\infty}^{\infty} (\mp 1)^{n+m} \frac{1}{-(t-t')^2 + [x-(-1)^n x' + na]^2 + [y-(-1)^m y' + ma]^2 + (z-z')^2 + i\epsilon}, \tag{3}$$

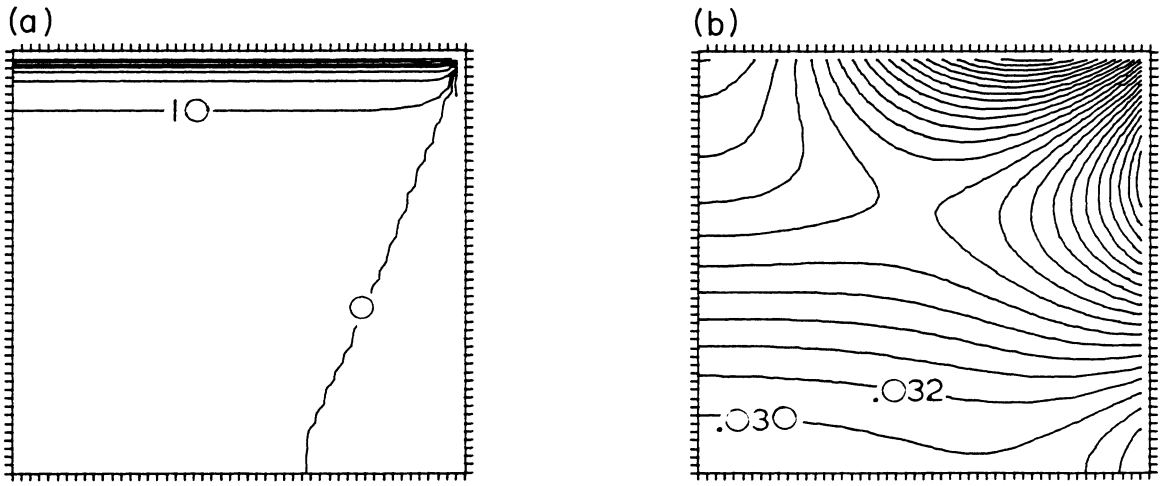

FIG. 9. As in Fig. 4, but for $\langle 0 \mid T^{xx} \mid 0 \rangle$ for the minimally coupled field satisfying Dirichlet boundary conditions.

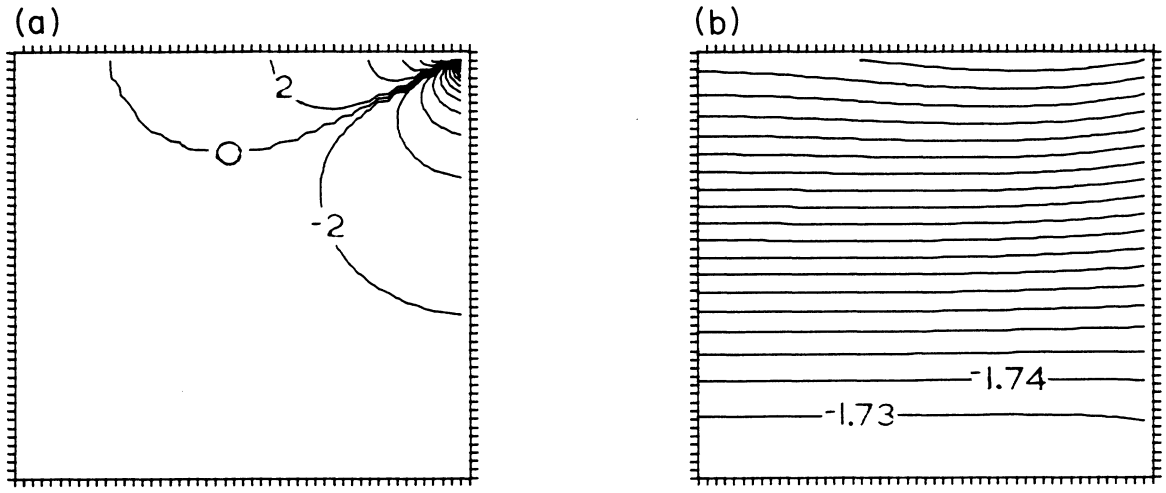

FIG. 10. As in Fig. 4, but for $\langle 0 | T^{xx} | 0 \rangle$ for the conformally coupled field satisfying Neumann boundary conditions.

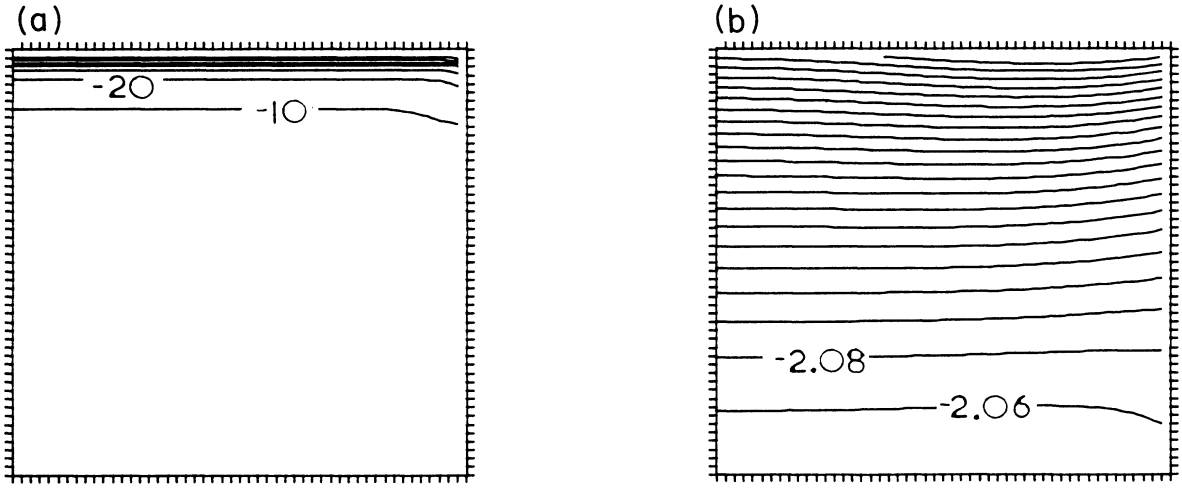

FIG. 11. As in Fig. 4, but for $\langle 0 | T^{xx} | 0 \rangle$ for the minimally coupled field satisfying Neumann boundary conditions.

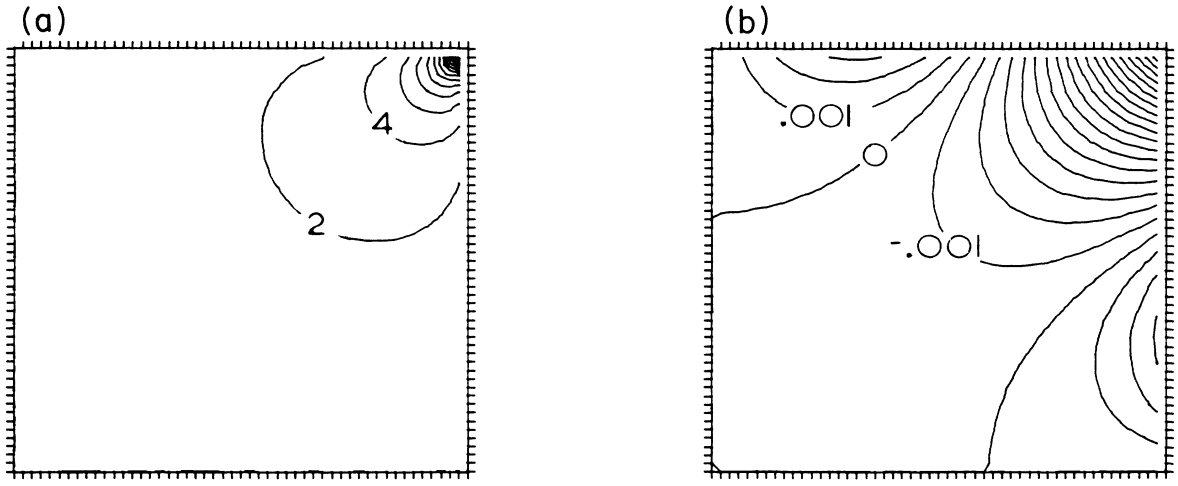

FIG. 12. As in Fig. 4, but for $\langle 0 | T^{xy} | 0 \rangle$ for the conformally coupled field satisfying either Dirichlet or Neumann boundary conditions.

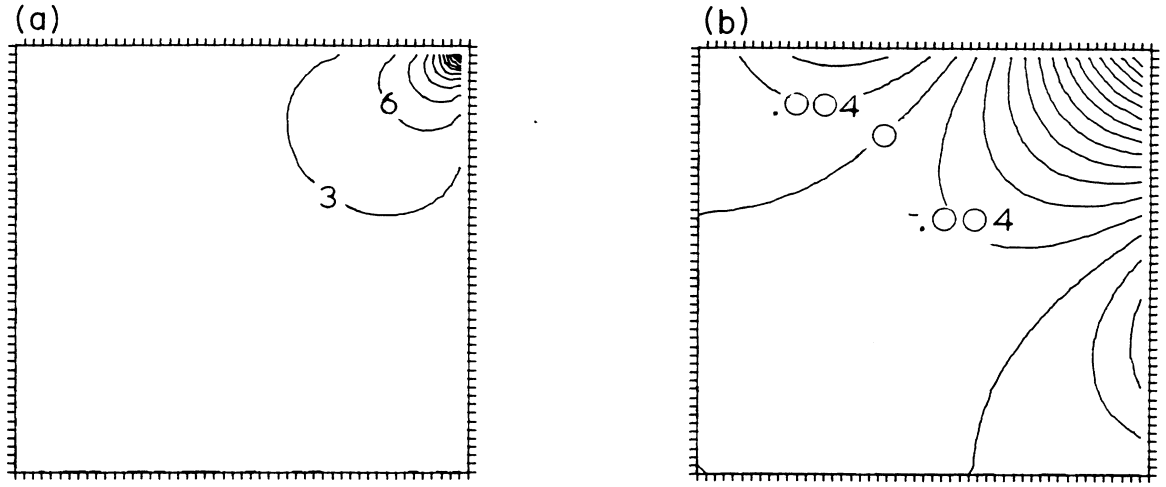

FIG. 13. As in Fig. 4, but for $\langle 0 | T^{xy} | 0 \rangle$ for the minimally coupled field satisfying either Dirichlet or Neumann boundary conditions.

where the sums are over the images shown in Fig. 3. The sums in $\langle 0 | T^{\mu\nu} | 0 \rangle_{D,N}$ cannot be done in closed form, however they are computed numerically to four figures of accuracy (n and m running from -50 to 50). The results are graphed in Figs. 4—13. Tables of numerical results may be obtained from the author. As expected we see corner divergences for the conformally coupled case and both edge and corner divergences for the minimally coupled case. In order to display the behavior of the stress tensor near the center of the box, these divergences have been subtracted (i.e., the contribution from the nine terms with $n=0, \pm 1$ while $m=0, \pm 1$). This subtracted result is plotted in Figs. 4(b)—13(b) next to the complete result.

III. THE ROTATING BOX

Consider the same manifold as was used in the previous section for the nonrotating box (see Fig. 3); but now with two different metrics, $\eta_{\mu\nu}$ and $g_{\mu\nu}$, where $g_{\mu\nu}$ differs from $\eta_{\mu\nu}$ by terms which are small. Then the Green's functions for the two spacetimes satisfy the equations

$$FG(x,x') = -g^{-1/2}\delta^4(x,x') ,$$

$$F_0 G_0(x,x') = -\eta^{-1/2}\delta^4(x,x') ,$$

where the subscript zero refers to quantities in the spacetime with metric $\eta_{\mu\nu}$ and the unsubscripted symbols refer to quantities in the spacetime with metric $g_{\mu\nu}$. Assume the Green's functions obey the same boundary conditions (either Dirichlet or Neumann). Left multiply the first equation by G_0, the second equation by G, and integrate over the spacetime manifold. Subtract, integrate by parts, and use the boundary conditions to obtain

$$\delta G(x,x') = \int d^4x'' G_0(x,x'')\delta F'' G_0(x'',x') , \tag{4}$$

where by definition

$$\delta G(x,x') = G(x,x') - G_0(x,x') \tag{5}$$

and

$$\delta F'' = F'' - F_0'' .$$

Thus we can obtain $G(x,x')$ from Eqs. (4) and (5). Let $g_{\mu\nu}$ be the metric appropriate to a Cartesian coordinate system rotating clockwise in the (x,y) plane about the origin, to first order in the angular velocity Ω, i.e.,

$$g_{\mu\nu} \simeq \begin{bmatrix} -1 & y\Omega & -x\Omega & 0 \\ y\Omega & 1 & 0 & 0 \\ -x\Omega & 0 & 1 & 0 \\ 0 & 0 & 0 & 1 \end{bmatrix} .$$

Now using the Green's function obtained in the previous section for the nonrotating box as $G_0(x,x')$ and using

$$\delta F'' = 2\Omega(y''\partial_{x''}\partial_{t''} - x''\partial_{y''}\partial_{t''})$$

we obtain an approximation, to first order in the angular velocity Ω, for the Green's function of a rotating box. The resulting expression for $\delta G(x,x')$ has four infinite sums and an integral over the entire spacetime region of the manifold and is not expressible in closed form. As we are ultimately interested in $\langle 0 | T^{\mu\nu} | 0 \rangle_{D,N}$ and not in $G(x,x')$ we go ahead and apply the differential operator of Eq. (2) to $G_0(x,x') + \delta G(x,x')$. The only components which contain a first-order correction to the results for the nonrotating box are $\langle 0 | T^{tx} | 0 \rangle_{D,N}$ and $\langle 0 | T^{ty} | 0 \rangle_{D,N}$. We obtain

$$\langle 0|T^{tx}|0\rangle_{D,N}=\lim_{x'\to x}(\{-y[(\tfrac{1}{2}-2\xi)(-\partial_t\partial_{t'}+\partial_x\partial_{x'}+\partial_y\partial_{y'}+\partial_z\partial_{z'})+(1-2\xi)(\partial_t\partial_{t'}-\partial_x\partial_{x'})$$
$$-\xi(\partial_{t'}\partial_{t'}+\partial_t\partial_t-\partial_{x'}\partial_{x'}-\partial_x\partial_x)]$$
$$-x[\tfrac{1}{2}(1-2\xi)(\partial_x\partial_{y'}+\partial_{x'}\partial_y)+\xi(\partial_{x'}\partial_{y'}+\partial_x\partial_y)]+\xi(\partial_{y'}+\partial_y)\}(-i)G_0(x,x') \quad (6a)$$
$$+\{-\tfrac{1}{2}(1-2\xi)(\partial_t\partial_{x'}+\partial_{t'}\partial_x)+\xi(\partial_{t'}\partial_{x'}+\partial_t\partial_x)\}(-i)\delta G_{D,N}(x,x')) \quad (6b)$$

as measured by an observer in the rotating frame. ($\langle 0|T^{ty}|0\rangle_{D,N}$ can be obtained from $\langle 0|T^{tx}|0\rangle_{D,N}$ by symmetry arguments and hence is not computed here.

By transforming the tensor $\langle 0|T^{\mu\nu}|0\rangle$ to the nonrotating system, we obtain

$$\langle 0|T^{tx}|0\rangle_{\text{nonrot}}=\langle 0|T^{tx}|0\rangle-y\Omega\langle 0|T^{00}|0\rangle$$

as the momentum density measured by an observer in the nonrotating frame. The difference between the momenta measured by the two observers is just what one would obtain by looking at the nonrotating energy in the rotating frame.

The stress-energy tensor in Eq. (6) is not as easy to regularize as the cases of Sec. II. Christensen[12] has calculated the general form for the infinities in the stress-energy tensor for any metric by the method of geodesic point splitting. Only the quartic divergence in his general expression appears in flat spacetimes, i.e.,

$$\langle 0|T^{\mu\nu}|0\rangle_\infty=\frac{g^{1/2}}{2\pi^2}\frac{1}{(\sigma^\rho\sigma_\rho)^2}\left[g^{\mu\nu}-4\frac{\sigma^\mu\sigma^\nu}{(\sigma^\rho\sigma_\rho)}\right],$$

where $\sigma(x,x')$ is the geodesic interval between x and x'.

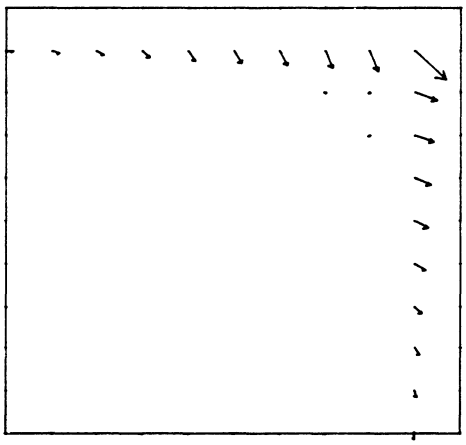

FIG. 14. The vacuum expectation value of the momentum density ($\langle 0|T^{tx}|0\rangle$ and $\langle 0|T^{ty}|0\rangle$ plotted as a vector) in units of $\Omega/4\pi^2a^3$, for the conformally coupled massless scalar field satisfying Dirichlet boundary conditions, confined inside an infinitely long rotating box with side of length a, centered at the origin, as measured by an observer in the nonrotating frame. The box is rotating clockwise. Plotted are the results for the upper right quadrant of a cross section of the box ($0\le x\le a/2$, $0\le y\le a/2$, $z=0$). Results for other quadrants can be obtained by successive rotations of $\pi/2$ about the origin.

We split points in the z direction so that $\sigma=\frac{1}{2}(z-z')^2$ giving

$$\langle 0|T^{\mu\nu}|0\rangle_\infty=\frac{1}{2\pi^2}\frac{1}{(z-z')^4}\times\begin{pmatrix}-1 & y\Omega & -x\Omega & 0\\ y\Omega & 1 & 0 & 0\\ -x\Omega & 0 & 1 & 0\\ 0 & 0 & 0 & -3\end{pmatrix}.$$

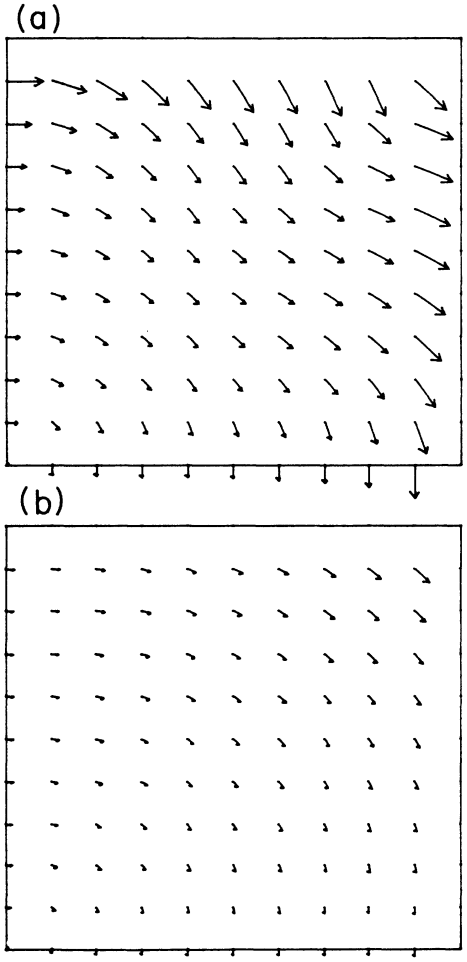

FIG. 15. (a) As in Fig. 14, but the lengths of the vectors have been scaled by taking eighth roots in order to show the direction of flow near the origin. (b) As in (a), but for just the nonrotating energy density $\langle 0|T^{tt}|0\rangle$ as observed in the rotating frame.

The term with $n=m=0$ in $G_0(x,x')$ makes a contribution of

$$\langle 0 | T^{tx} | 0 \rangle_\infty = \frac{y\Omega}{\pi^2(z-z')^4}$$

to the divergence in $\langle 0 | T^{tx} | 0 \rangle_\infty$, twice the expected result. This means that part of the divergence must come from $\delta G(x,x')$. In fact the extra part of the divergence comes from the $n=n'=m=m'=0$ term in $\delta G(x,x')$. To see this we evaluate this term, using the method described in the Appendix for the general terms, with the exception of a change in the ranges of the x'' and y'' integrals. Since the expected divergence is a part of the usual Minkowski divergence (i.e., from the entire Minkowski spacetime) we extend the x'' and y'' integrals from minus infinity to infinity and then subtract the integral outside the spacetime manifold to obtain the original integral over the inside of the spacetime manifold. The extended integral gives precisely the missing piece of the divergence and is thrown away in the renormalization procedure. The subtracted integral over the outside of the box is then a contribution to the finite part of the stress-energy tensor and must be included in our calculation.

The first term in Eq. (6a) was evaluated numerically to four figures of accuracy by summing n and m from -50 to 50. The numerical evaluation of the second term in Eq. (6b) is discussed in the Appendix. Tables of numerical results may be obtained from the author. Figures 14—18 show $\langle 0 | T^{tx} | 0 \rangle$ and $\langle 0 | T^{ty} | 0 \rangle$ plotted as vectors to show both the magnitude and direction of the momentum density as seen by an observer in the nonrotating frame. Below these are plotted the results for the zeroth-order energy density as seen by an observer in the rotating frame. (Recall that to get the momentum density as seen by an observer in the rotating frame, these two graphs should be added.) Notice that the momentum density is always much larger than just the zeroth-order energy density as seen by the rotating observer. Also notice that the momentum density blows up near the edges of the box even in the conformally coupled case. This is because the boundaries are curved in a spacetime sense.

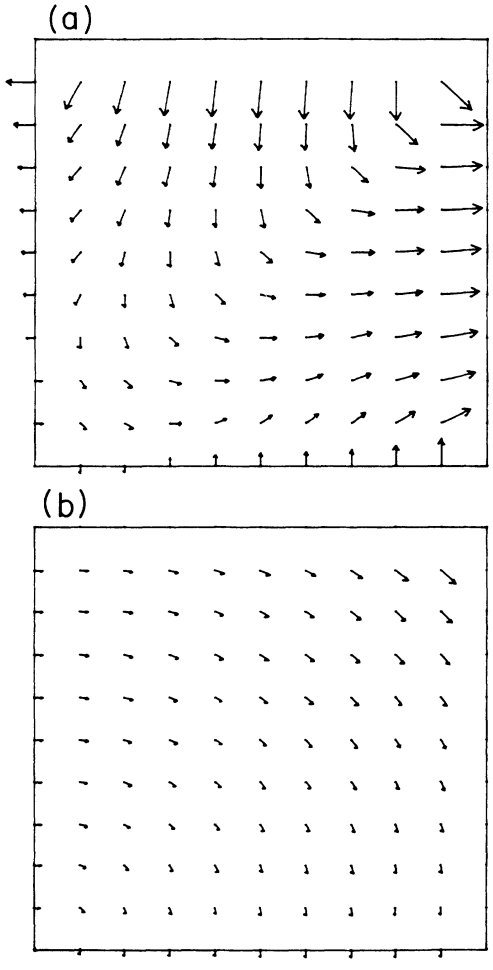

FIG. 16. As in Fig. 15, but for the conformally coupled field satisfying Neumann boundary conditions.

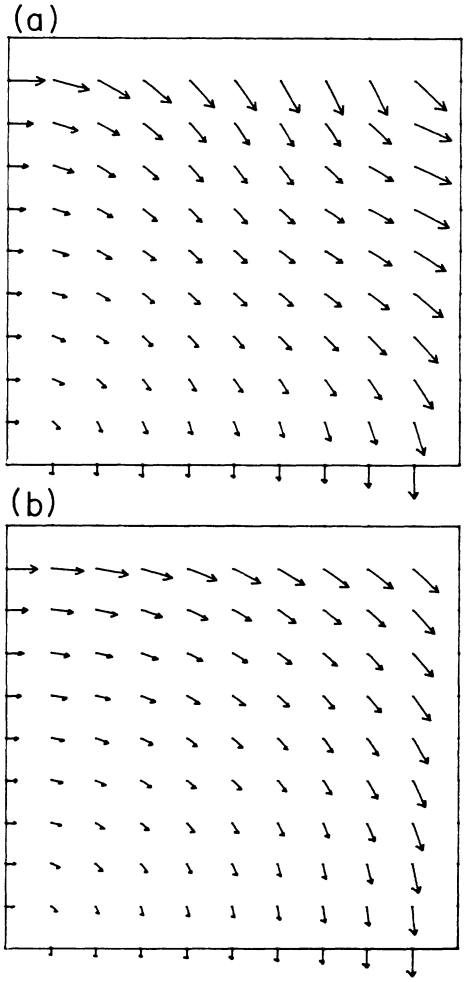

FIG. 17. As in Fig. 15, but for the minimally coupled field satisfying Dirichlet boundary conditions.

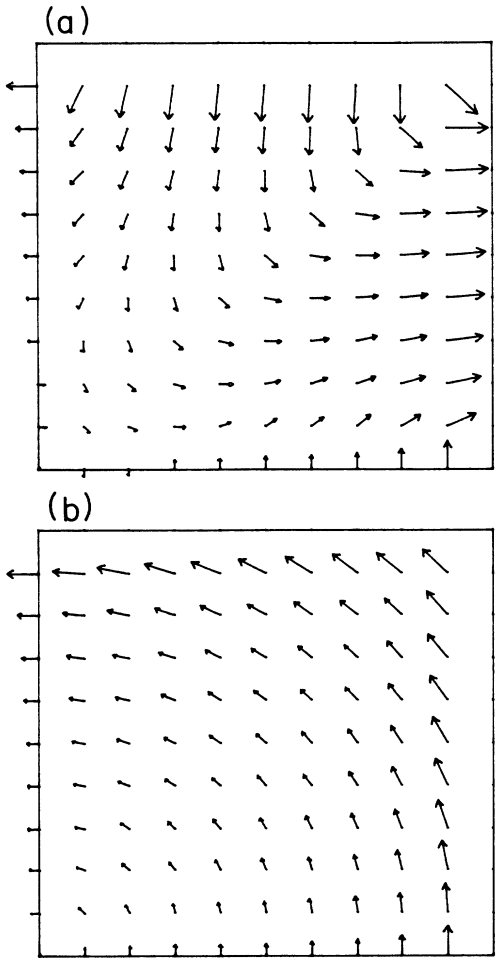

FIG. 18. As in Fig. 15, but for the minimally coupled field satisfying Neumann boundary conditions.

It is possible to obtain a rough estimate of the moment of inertia per unit length for a box. Using our results for the momentum density, we make a Riemann sum type estimate for the total angular momentum density. Since we have no results on the edge of the box, this results in an effective cutoff at wavelengths on the order of one-hundredth the size of the box. Dividing the total angular momentum by the angular velocity, we obtain for the moment of inertia per unit length

$$I=\frac{8000}{4\pi^2}\frac{\hbar}{c}\ .$$

Notice that the answer is proportional to $\hbar/c$ (very small) and independent of the cross-sectional size of the box. Obviously our rough estimate is physically unrealistic in that the cutoff scales with the size of the box. A physically realistic box would have a cutoff depending on the molecular details of the boundary material introducing another length scale into the problem. Assume that the momentum diverges inversely as the distance from the edge or corner of the box to the inverse fourth power. We use the numerical data near the edge of the box to fit the overall proportionality constants and integrate over the edges and corners of the box where we have no numerical data. The corner contributions are the largest giving a constant piece which approximately cancels the first estimate and an additional term

$$I\simeq\frac{50}{4\pi^2a^3}\frac{\hbar}{c}\frac{1}{\rho^2}\ ,$$

where $\rho=$the interatomic spacing/the size of the box. Even with $\rho\simeq10^{-10}$, and $a\simeq1$m, we obtain $I\simeq10^{-22}$ kg m, still extremely small.

ACKNOWLEDGMENTS

It is a great pleasure to thank B. S. DeWitt and P. Candelas for their many helpful discussions throughout the course of this work. I gratefully acknowledge financial support from the American Association of University Women and National Science Foundation Grant No. PHY 8205717.

APPENDIX

In this appendix we give an outline of how to evaluate the second term Eq. (6b) where

$$\delta G(x,x')=\int d^4x''G_0(x,x'')(2\Omega)(y''\partial_{x''}\partial_{t''}-x''\partial_{y''}\partial_{t''})G_0(x,x')$$

with

$$G_0(x,x')=\frac{i}{4\pi^2}\sum_{n=-\infty}^{\infty}\sum_{m=-\infty}^{\infty}(\mp1)^{n+m}\frac{1}{-(t-t')^2+[x-(-1)^nx'+na]^2+[y-(-1)^my'+ma]^2+(z-z')^2+i\epsilon}\ .$$

First take the derivatives indicated in Eq. (6). (Judicious use of integration by parts at this stage will make succeeding equations look simpler and more symmetric.) Combine the factors in the denominators using the Feynman integral

$$\frac{1}{a^3b^3}=\int_0^1 du\frac{u^2(1-u)^2}{[a(1-u)+bu]^6}\ .$$

The t'' and z'' integrals are straightforward using standard techniques, leaving four infinite sums (over n, n', m,

m') and three finite integrals (over x'', y'', and u) to be evaluated. For simplicity rescale the x'' and y'' integrals to factor the length of the box out of the integrand. Regularize the result as indicated in Sec. III and renormalize by throwing away the Minkowski divergence. Take the limit $x' \to x$ in the finite remainder.

As this stage the problem breaks into several pieces. In the terms where $n = n'$ and $m = m'$ all of the integrals can be evaluated in closed form leaving just a double sum to be evaluated numerically. Take the sums from $n, m = -50$ to 50 to obtain four figures of accuracy. The term with $n = n' = m = m' = 0$ is similar but the x'' and y'' integrals extend over the outside of the box instead of the inside as discussed in the regularization procedure of Sec. III.

The terms with $n \neq n'$ and $m \neq m'$ are the most complicated. The u integral can be evaluated in closed form leaving

$$\frac{-3\Omega}{\pi^3 a^3} \sum_{\substack{n \neq n' \\ m \neq m'}} (-1)^{n+n'+m+m'} \int_{-1/2}^{1/2} dx'' \int_{-1/2}^{1/2} dy'' \left[\frac{1}{3AD(D-A)^2} + \frac{4}{(D-A)^4} + \frac{2(D+A)}{(D-A)^5} \ln \frac{A}{D} \right]$$

$$\times (y''[(-1)^n + (-1)^m][x'' - (-1)^n x + n)(x'' - (-1)^{n'} x + n']$$

$$- x''\{(-1)^{n'}[x'' - (-1)^{n'} x + n'][y'' - (-1)^m y + m]$$

$$+ (-1)^n [x'' - (-1)^n x + n][y'' - (-1)^{m'} y + m']\}) , \tag{A1}$$

where

$$A = [x'' - (-1)^n x + n]^2 + [y'' - (-1)^m y + m]^2, \quad D = [x'' - (-1)^{n'} x + n']^2 + [y'' - (-1)^{m'} y + m']^2 ,$$

At this point we are left with four nested sums and two integrals to evaluate numerically. If each sum or integral requires a mere ten terms to converge sufficiently, we have to make 10^6 evaluations of the integrand for each spacetime point at which we wish to evaluate the stress-energy tensor. Clearly computational speed is more important than elegance if an answer is desired in finite computer time.

An eleventh-degree two-dimensional Gaussian routine with minimal (28) points[13] (not a simple product rule) is used to evaluate the x'' and y'' integrals. Successive iterations can be obtained by dividing the box up into smaller squares and using the Gaussian rule on each of the smaller squares. The number of squares is increased until the convergence necessary to ensure three-figure accuracy in the sums is assured. Then the sums over n, n', m, and m' are done symmetrically out from zero until three-figure accuracy is attained. Near the edges of the square, convergence of the integrals is very slow, but fortunately the convergence of the sums is extremely rapid, only the first few terms contributing to the desired accuracy. Near the center of the square convergence of the integrals is extremely rapid with one to three iterations giving ten-figure accuracy, but the sums converge slowly and need to be extended to much higher values. (Convergence was checked only for representative terms in the various areas in order to obtain necessary speed in the routine.) Special care is necessary in two special cases where the integrand in Eq. (A1) might diverge, i.e., when A or D equals zero, and when A equals D.

Case 1: A or $D = 0$. This can only happen if n and m are both zero or if n' and m' are both zero. In these cases the possible singularity occurs at the single point $x'' = x$, $y'' = y$. To examine the behavior of the integrand at this point, change variables to $x'' = x + r\cos\theta$, $y'' = y + r\sin\theta$, and expand the integrand for small r. Find that while it is true that the integrand diverges at the point $r = 0$, the integral in a small circle around that point is finite. To handle this situation during the numerical integration it is important to choose points at which the integrand is evaluated symmetrically about this singularity and of course not on the singularity. (For this reason it was decided to evaluate the stress-energy tensor at intervals of $0.05a$ inside the box. The number of iterations of the numerical integration routine was then carefully chosen to ensure that the points at which the integrand was evaluated were symmetric about the singularity. It was also verified by explicit calculation in some representative cases that the answers from the numerical routine were not significantly at odds with the results from an analytic calculation in a small region around the singularity.)

Case 2: $A = D$. A equals D along a straight line in the (x'', y'') plane which may or may not cross through the region of integration, depending on the values of n, n', m, and m'. To examine the behavior of the integrand along this line, make a change of variables, to u which lies along the line and v which is perpendicular to it. An expansion of the integrand for small values of v shows that in fact

the integrand is finite along this line although the individual terms in the integrand are not. (During the numerical integration, the zeroth-order value of the expansion was used to evaluate the integrand whenever one of the points at which the integrand was to be evaluated fell on third line. Checks were made that points near but not on the line did not introduce significant error.)

---

*Present address: Department of Mathematical Sciences, University of Durham, Durham, DH1 3LE, England.

[1]H. B. G. Casimir, Proc. Kon. Ned. Akad. Wetenschap. **51**, 793 (1948) [Indag. Math. **10**, 261 (1948)].

[2]M. J. Sparnaay, Physica **24**, 751 (1958).

[3]D. Deutsch and P. Candelas, Phys. Rev. D **20**, 3063 (1979); J. S. Dowker, quoted therein.

[4]In particular for a spherical shell see T. H. Boyer, Ann. Phys. (N.Y.) **56**, 474 (1970).

[5]D. Deutsch and P. Candelas, Phys. Rev. D **20**, 3063 (1979).

[6]P. Candelas, Ann. Phys. (N.Y.) **143**, 241 (1982).

[7]In two space-time dimensions, the problem was first solved by S. A. Fulling, Phys. Rev. D **7**, 2850 (1973). In four space-time dimensions, the problem was first solved by P. Candelas and D. Deutsch, Proc. R. Soc. London **A354**, 79 (1977); **A362**, 251 (1978).

[8]J. R. Letaw and J. D. Pfautsch, J. Math. Phys. **23**, 425 (1982); J. D. Pfautsch, Phys. Rev. D **24**, 1491 (1981).

[9]I. S. Gradshteyn and I. M. Ryzhik, *Tables of Integrals, Series, and Products* (Academic, New York, 1965), p. 981.

[10]See, for example, B. S. DeWitt, Phys. Rep. **19C**, 295 (1975).

[11]L. S. Brown and G. J. Maclay, Phys. Rev. **184**, 1272 (1969).

[12]S. M. Christensen, Phys. Rev. D **14**, 2490 (1976).

[13]A. H. Stroud, *Approximate Calculations of Multiple Integrals* (Prentice-Hall, New Jersey, 1971), p. 259.